Title: Morphology, but not microtubules, of the retinal nerve fibers are protected by nicotinamide in glaucoma mice

Authors: Vinessia Boodram[1] and Hyungsik Lim[1,2]

[1]Department of Physics and Astronomy, Hunter College of the City University of New York, New York, NY 10065

[2]School of Optometry, Indiana University, Bloomington, IN 47405

Correspondence should be addressed to Hyungsik Lim, hl128@iu.edu

Abstract:

Glaucoma is a blinding disease where the retinal ganglion cells (RGCs) and the axons degenerate. Degradation of axonal microtubules is thought to play a critical role in the pathogenesis, but the mechanism is unknown. Here we investigate whether microtubule disruption in glaucoma can be alleviated by metabolic rescue. Using nicotinamide to reduce metabolic stress, the morphology and integrity of microtubules of the retinal nerve fibers are examined in a mouse model of glaucoma, DBA/2. Surprisingly, we found that morphology but not microtubules are protected by the dietary supplement of nicotinamide. Co-registered second-harmonic generation and immunofluorescence images shows that microtubule deficit is not due to a shortage of tubulins and colocalizes with the sectors in which RGCs are disconnected from the brain, indicating that the instability of axonal microtubules may underlie axonal transport deficit in glaucoma. Together, our data confirms distinct roles of axonal microtubules in glaucomatous degeneration, offering a new opportunity for neuroprotection.

Keywords: retina; glaucoma; retinal ganglion cell; axon; microtubule; second harmonic generation; metabolism

Significance Statement: Glaucoma is one of the leading causes of blindness worldwide, but the lack of understanding on the molecular mechanism hinders the development of cure. Here the significance of axonal microtubules in the RGCs is investigated, i.e., whether it depends on metabolic decline common in the aging retina. We found that nicotinamide, a promising neuroprotective agent alleviating metabolic stress, does not protect axonal microtubules as effectively as the morphology of the retinal nerve fibers. Our data also suggests multiple independent modes of protective action by nicotinamide. Overall, our results support a crucial role of axonal microtubules in the progressive loss of RGCs in glaucoma, promoting the feasibility of novel neuroprotective strategies.

1. Introduction

Glaucoma is a leading cause of blindness worldwide[1,2]. Nearly half of the retinal ganglion cells (RGCs) and their axons are irreversibly lost by the time of diagnosis. The risk factors include aging and high intraocular pressure (IOP), but the pathogenic mechanism is poorly understood hampering the prevention of vision loss. Axonal microtubules have been postulated to play an important role in the disease[3-5]. It has been demonstrated that in DBA/2 (DBA) mice, a well-characterized model of inherited glaucoma[6-9], axonal microtubules decay with age more rapidly than the RGC axons (i.e., the retinal nerve fibers)[10]. The degradation of microtubules would impair axonal transport depriving the RGCs of essential tropic and metabolic supports. One of the possible drivers of the loss of microtubules is dysfunctional cellular metabolism, which could compromise active regulations stabilizing the microtubule lattice. Microtubule stability and metabolic equilibrium are co-dependent: Conversely, the disturbance of microtubules, which enable intracellular transport of mitochondria, could induce local energetic shortfall in the distal compartments. Lowering metabolic stress with metabolites, e.g., nicotinamide adenine dinucleotide (NAD) or its precursor nicotinamide (NAM), has been demonstrated to delay or halt axonal degeneration[11] and protect RGCs against glaucoma[12,13]. It is plausible that the mechanism of neuroprotection by NAD/NAM involves axonal microtubules. Here, using NAM as a paradigm, we investigate how axonal microtubules of RGCs respond to metabolic rescue.

2. Results

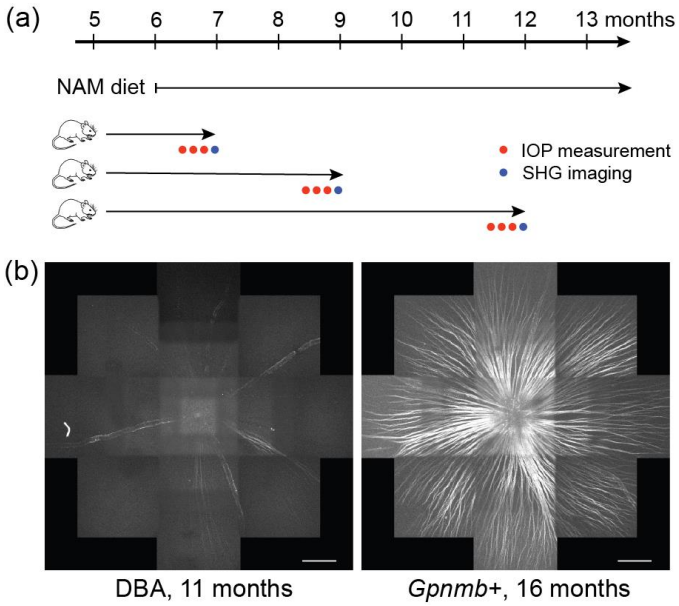

Fig. 1. Overview of experiment. (a) Timeline of measurements. (b) Degenerated DBA and healthy *Gpnmb*+ retinas visualized by SHG. Scale bars, 300 μm.

NAM protects morphology of the retinal nerve fibers. An overview of the experiment is shown in Fig. 1(a). A group of DBA mice received a dietary supplement of NAM prophylactically from 6 months of age at a low dose of 550 mg of body weight per day, as previously demonstrated[12,13]. As a control, another group of DBA mice received a normal diet without NAM at the same ages.

The strain-matched, homozygous *Gpnmb*+ mice (DBA-*Gpnmb*+) were used as a non-glaucomatous control[14]. At a desired age, the IOP was measured using a TonoLab tonometer[15] on three different dates prior to imaging, and the average was taken. Second-harmonic generation (SHG) microscopy was performed for measuring the amount of microtubules in the retina nerve fibers[16,17]. Unlike immunofluorescence probing the unit proteins, i.e., tubulins, SHG signal is sensitive to uniform polymers[18], therefore ideal for studying axonal microtubules in the functional form. Mosaics were acquired over a region on and around the optic nerve head. Image processing was carried out to normalize the SHG intensity and evaluate the thickness of the retinal nerve fibers[10]. Then, the normalized SHG intensity divided by thickness, namely SHG density, provides a relative measure of the density of axonal microtubules at a microscopic resolution. The mean SHG density was evaluated as an average over the retinal nerve fibers in the mosaic.

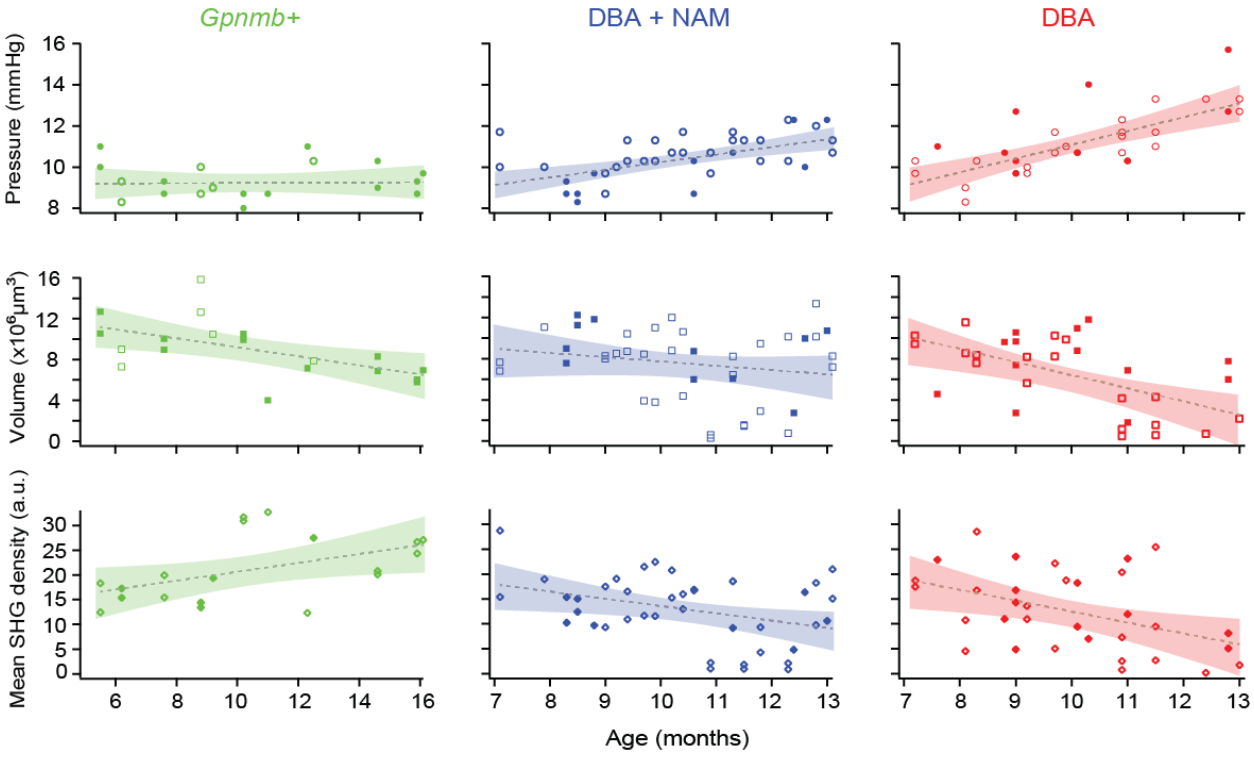

Fig. 2. Effects of NAM dietary supplement on the DBA retinas. The IOP, volume, and mean SHG density of the retinal nerve fibers are shown for three groups, i.e., *Gpnmb*+ and DBA with and without NAM diet. Solid and open markers are male and female, respectively. Dashed lines with shaded bands are linear regressions with 95% confidence bounds.

The effect of NAM diet is summarized in Fig. 2. The animal-to-animal variations of DBA mice were a bit larger than the variations of *Gpnmb*+ data which are primarily due to the experimental errors. The IOP of the *Gpnmb*+ eyes remained stable (N=19, 13 from 8 males and 6 from 4 females) and that of the control DBA eyes without NAM diet increased with age (N=33, 13 from 8 males and 20 from 12 females), as expected. However, the rate of IOP increase with age in the NAM-treated DBA eyes (N=41, 11 from 8 males and 30 from 16 females) was significantly diminished compared to the control DBA ($p<0.01$, a linear regression model with interaction between age and diet). Dampened IOP elevation with NAM has been also observed in the prior study but at a higher dose[12,13]. Other age-dependent changes of the retinal nerve fibers were also analyzed using a

linear regression model with interaction between age and diet. The benefits of the NAM supplement were significant, especially for protecting the morphology. The DBA group with NAM diet had its volume significantly better preserved against age-dependent loss compared to the no-NAM DBA controls ($p<0.05$). The decay of mean SHG density was also slower with NAM diet, but it was not statistically significant ($p=0.37$).

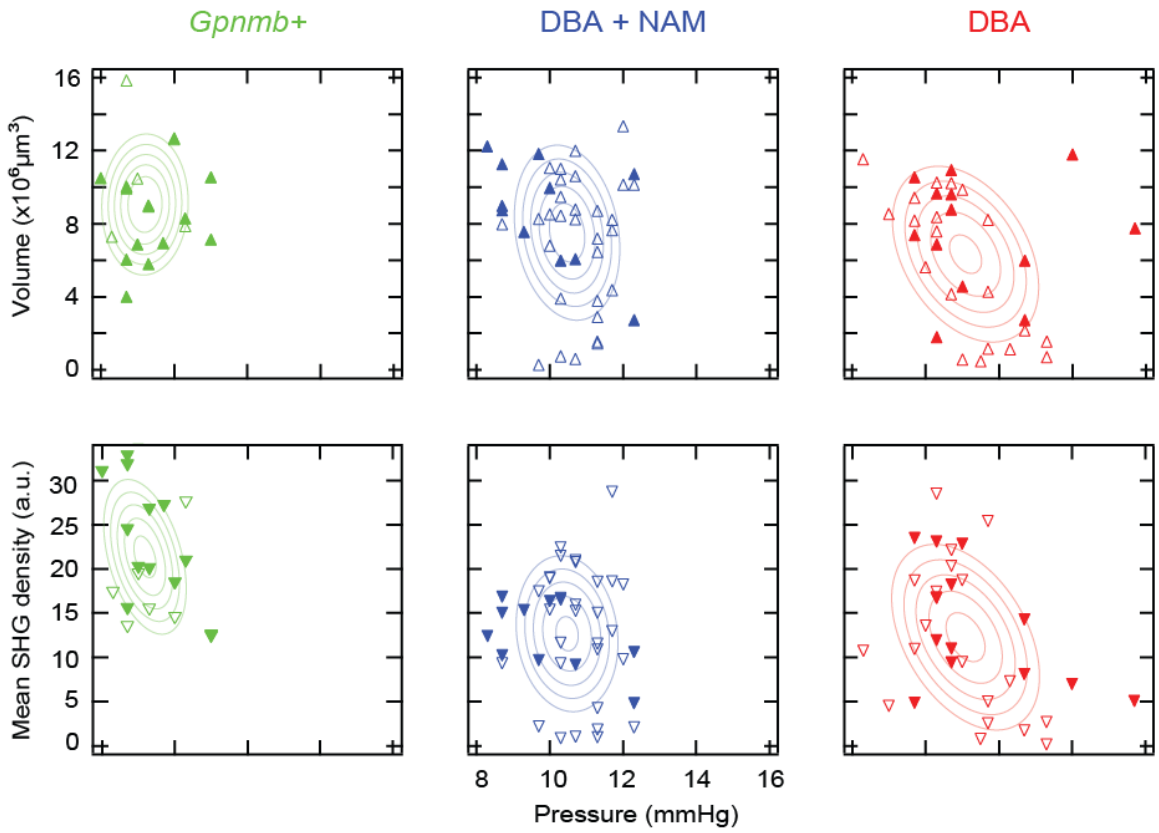

Fig. 3. Correlation between morphology and microtubules versus IOP for three groups. Solid and open markers are male and female, respectively, overlaid with the best fits to the bivariate normal distribution.

The protective effects of NAM may be partially mediated by reduced ocular hypertension. A question was raised whether the benefit of NAM in protecting the retinal nerve fibers was a consequence of the decreased IOP, instead of being a direct effect of bolstered metabolism. To investigate this, we examined the correlation coefficients between the properties of the retinal nerve fibers versus the IOP (Fig. 3). It was anticipated that, if the protection of the volume by NAM was entirely mediated by the IOP reduction, the correlation between the parameter and the IOP will be unchanged by NAM. For the DBA group without NAM diet, there was a modest negative correlation between the volume and the IOP (Pearson correlation coefficient $r=-0.37$, $p<0.05$). For the DBA group with NAM diet, however, the correlation could not be determined with confidence (Pearson correlation efficient $r=-0.19$, $p=0.24$), thus unable to reject a scenario where NAM has an additional mode of action to prevent the loss of RGC axons. There was also a moderate negative correlation at the level of significance between the mean SHG density and the IOP for the DBA group without NAM diet (Pearson correlation efficient $r=-0.42$, $p<0.05$). The disruption of

axonal microtubules, like the eventual loss of RGC axons, is likely to be a downstream effect of the IOP elevation.

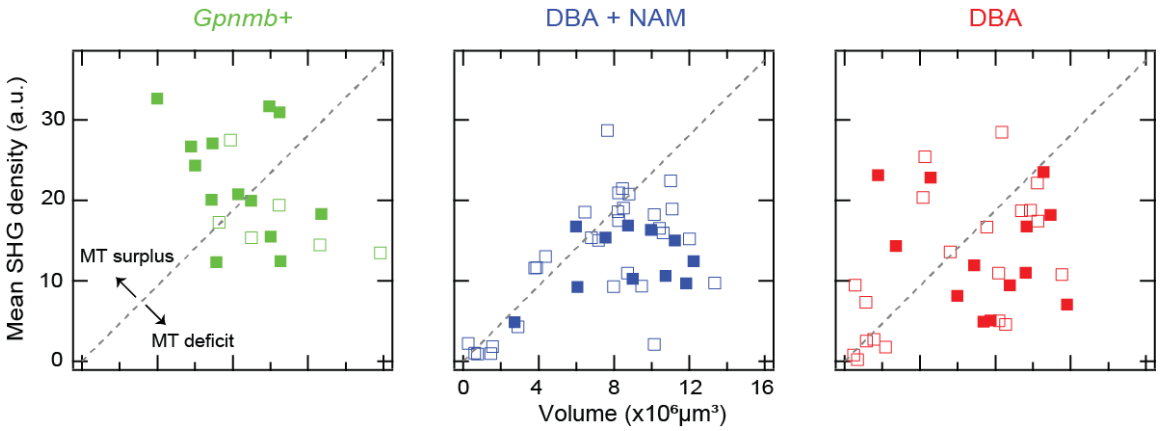

Fig. 4. Differential response of morphology and microtubules to NAM. MT; microtubule. Solid and open markers are male and female, respectively. Dashed line, the average slope of the *Gpnmb*+ retinas.

NAM improves morphology more effectively than microtubules of the retinal nerve fibers. Axonal microtubules are disrupted before the loss of RGC axons during glaucomatous degeneration, leading to a pathological state called *microtubule deficit*[10]. We asked if the deficit is aggravated by declined metabolism rendering axonal microtubules unstable. The hypothesis predicts that microtubule deficit will be mitigated by NAM supplement. To test this idea, we analyzed the mean SHG density and the volume of the NAM- versus non-treated DBA retinas. Microtubule deficit, i.e., a less than normal ratio of mean SHG density to volume, was assessed by comparing the two properties in the same retinas (Fig. 4). The deficit of the control DBA retinas relative to the *Gpnmb*+ control was apparent, reproducing with a different set of instruments the previous findings[10]. It confirms microtubule deficit as a molecular marker of glaucoma. By contrast, an unexpected result was obtained from the NAM-treated DBA retinas, i.e., deficit became more severe than the control DBA retinas. It was due to the differential response to NAM, i.e., that the morphology of the retinal nerve fibers, but not microtubules, was significantly improved with NAM diet, as already shown in Fig. 2. The difference was even more recognizable in terms of microtubule deficit, i.e., when the two parameters are studied in the same retinas. The limited protection of axonal microtubules implies that the primary pathogenic source is independent of metabolic stress.

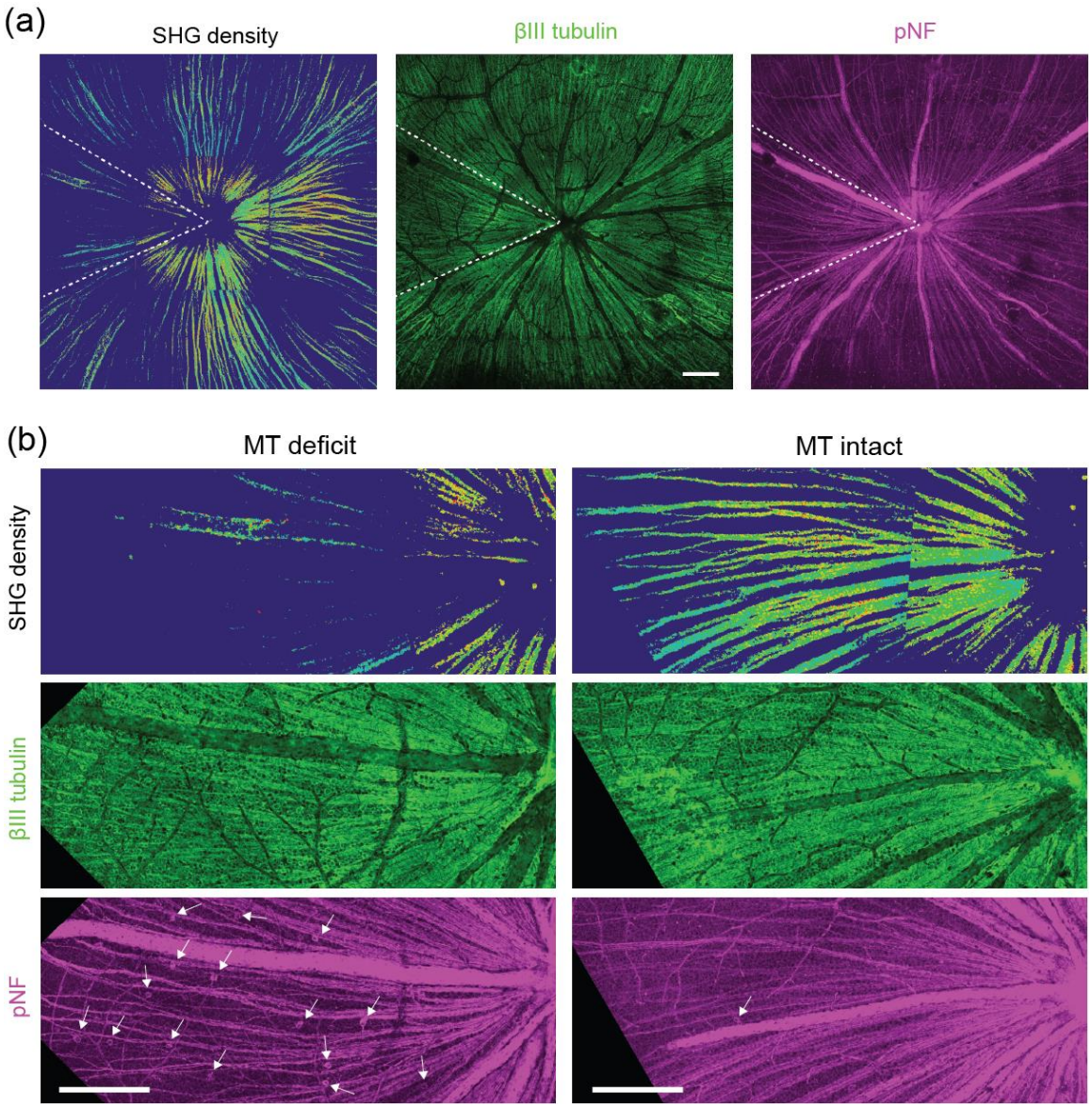

Fig. 5. Microtubule deficit versus the distribution of cytoskeletal proteins, βIII tubulin and pNF. (a) Mosaics of a DBA retina (22 months age, female) by SHG and immunofluorescence against the cytoskeletal elements. (b) Comparing two sectors with deficient and intact microtubules. Arrows, pNF+ RGC somas. Scale bars, 200 µm.

Microtubule deficit is not due to paucity of tubulins. Next, we asked whether microtubule deficit is due to a shortage of tubulin monomers, e.g., from inadequate expression or transport to the RGC axons, or a failure to stabilize the polymer, e.g., from dysfunctional regulation. To resolve these possibilities, we fixed the DBA retinas immediately after SHG imaging and double immunostained against cytoskeletal proteins, i.e., class III beta-tubulin (βIII) and phosphorylated neurofilament (pNF). The former is a neuron-specific isoform of tubulin. The latter is normally enriched in axons but accumulates in the soma of degenerating RGC's, which can be detected with a specific monoclonal antibody lacking nonspecific staining of soma (2F11). The somatic accumulation of pNF indicates that the RGC is disconnected from the brain, as validated with retrograde tracing[19,20]. Immunofluorescence was co-registered with SHG images to examine the

microtubule integrity and the abundance of tubulins in the same regions. A total of 12 DBA retinas were evaluated, primarily focusing on the age range between 10 and 12 months. In the retinas exhibiting pronounced sectorial degeneration (N=4), which is a characteristic in glaucoma pathology, the sectors of microtubule deficit always contained morphologically intact retinal nerve fibers (Fig. 5(a), between dashed lines). Also, it also showed high signals of βIII tubulins inside the sector, i.e., no substantial impairment in the expression or transport. It can be therefore concluded that microtubule deficit is likely due to the instability of microtubules rather than a low level of tubulins.

Loss of axonal microtubules colocalizes with the RGC's disconnect from the brain. SHG density was compared with the distribution of pNF to investigate the relationship between microtubule and transport deficits. In our observations, the retinas with pNF+ somas were infrequent and pNF+ somas represented a small subset of the RGC population (in the order of dozens in an area of approximately 1.8 mm diameter around the optic nerve head) (Fig. 5(b)). Furthermore, pNF+ somas were absent in highly degenerated areas (fig. S1). Presumably, not all RGCs undergo this pathological fate during glaucomatous degeneration and/or the redistribution of pNF is short-lived with pNF+ RGC somas disappearing altogether upon the cells' death. Interestingly, pNF+ RGC somas were also localized in sectors (Fig. 5 and fig. S1) and routinely coincided with that of low SHG density (Fig. 5(b)). It suggests that the RGC's connection to the brain is likely to be severed at the time of microtubule disruption while the RGC axons are intact, i.e., at the stage of microtubule deficit.

3. Discussion

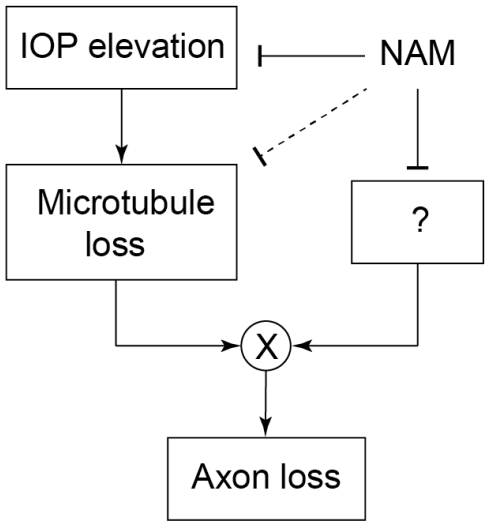

Fig. 6. Model of the glaucomatous degeneration of RGC axons.

NAM/NAD has multiple independent mechanisms to protect RGC axons. Taken together, our data supports a model in which NAM has independent modes of action targeting distinct aspects across the pathways of glaucoma pathogenesis (Fig. 6). The IOP elevation has a component that responds to NAM. While the reduced ocular hypertension seems to be partially responsible, there can be also an IOP-independent mechanism by which NAM protects the retinal nerve fibers, which is consistent with the previous finding that NAM protects RGCs without altering the IOP[12,13]. Specifically, NAM promotes the morphology of the retinal nerve fibers more significantly than microtubules. The differential response can be explained by theorizing that the loss of RGC axons is a compound effect of microtubule disruption and another necessary

condition downregulated under metabolic stress ('?' in Fig. 6). NAM/NAD controls diverse cellular processes in most cell types, thus it is also conceivable to affect more aspects of the RGC degeneration. Detailed knowledge of the distinct actions can provide a guide to improve the precision of NAM-based glaucoma therapy.

Axonal microtubules in the glaucomatous RGC degeneration. Here crucial insights have been achieved into the pathology of axonal microtubules in glaucoma. Microtubule deficit is not a consequence of a shortage of tubulins in the RGC axon. Metabolic stress, such as mitochondrial abnormalities or depletion of metabolites, was hypothesized to destabilize axonal microtubules. However, based on the relatively weak protection by NAM, microtubule disruption does not appear to be strongly related to metabolic decline. Instead, a major culprit could be the elevated IOP, which exhibits a negative correlation with axonal microtubules. Another important question is whether deteriorating axonal microtubules play a causal role in the eventual loss of RGCs. Our multimodal data reveals spatially overlapping, sectorial patterns of microtubule and axonal transport deficits. Correlated sectorial degenerations have allowed researchers to associate the loss of RGC axons with pathogenic insults at the optic nerve head[7,21-23]. Similarly, the aligned deficits of axonal transport and microtubules suggest that the cytoskeletal breakdown could be an intermediate stage in the progressive RGC death. The proposed role of axonal microtubules offers a new opportunity for neuroprotection against glaucomatous degeneration.

4. Methods

Animals. All procedures were approved by the Hunter College Institutional Animal Care and Use Committee (IACUC). DBA (DBA/2J, # 000671) and *Gpnmb*+ (DBA/2J-*Gpnmb*+/SjJ, # 007048) mice were obtained from The Jackson Laboratory and housed in the animal facility at Hunter College.

Pharmacology. Nicotinamide was given at a low dose of 550 mg of body weight per day[12,13] by adding to standard pelleted chow (2750 mg/kg) (Bio-Serv).

IOP measurement. IOP was measured using a TonoLab tonometer (Icare) while mice were awake (i.e., unanesthetized) and restricted. Three measurements were performed on consecutive dates prior to SHG imaging. The time of measurement was standardized at a fixed hour during daytime to avoid the intraday fluctuations[24].

Tissue preparation. The animal was deeply anesthetized with isoflurane and the first eye was enucleated. After the enucleation of the second eye, the animal was euthanized by CO_2 inhalation. The retinal flatmounts were prepared as previously described[10]. Briefly, an incision was made along the corneal limbus, the lens and sclera were removed, and radial cuts were made to relieve the curvature tension. The flat-mounted retina was transferred to a glass bottom dish (MatTek Corp.) and incubated at room temperature in the Ames' medium (A1420, Sigma-Aldrich) oxygenated with 95%O_2/5%CO_2.

SHG microscopy. An experimental setup for SHG microscopy was similar to the previous study[10,16]. Briefly, 100-fs pulses at an 80-MHz repetition rate from a Ti:Sapphire laser (Chameleon Ultra, Coherent, Inc.) were used for the excitation. The output wavelength was 900 nm. The polarization state of excitation beam was controlled with half- and quarter-waveplates. A water-dipping microscope objective lens (HC FLUOTAR L 25x 0.95NA, Leica) was used to focus the excitation beam onto the sample. The average power was approximately 20 mW at the sample. The forward-propagating SHG from the sample was collected with an UV-transparent high-NA objective lens (UApo340 40× 1.35NA, Olympus), passed through a narrow-bandpass filter (<20-nm bandwidth) at a half of the excitation wavelength (400 nm), and then detected with a photomultiplier tube (PMT; H7422-40, Hamamatsu, Inc.). Images with 512×512 pixels were

acquired, and the pixel dwell time was ~3 µs. A region was imaged twice for orthogonal linear polarizations, which then were summed into a composite image. Z-stacks were acquired in a step of 2 µm. For creating mosaics, a total of 9 regions (742x742 μm^2 each) were imaged on and around the optic nerve head at 1-mm radius.

Immunohistochemistry and confocal microscopy. Immunohistochemistry was performed similar to the prior studies[20,23]. After SHG imaging, the retinal flatmount was fixed with 4% paraformaldehyde for 20 minutes at room temperature. The sample was dehydrated sequentially in 25%, 50%, 75%, and 100% cold methanol for 15 min each and then permeabilized with dichloromethane for 2 hours. Then the retina was rehydrated in 75%, 50%, 25%, and 0% cold methanol for 15 min each. The sample was blocked in a buffer containing 5% normal serum and 0.3% Triton™ X-100 (Thermo Fisher Scientific, Inc.) for 3 hours. The sample was incubated in the primary antibody buffer at 4°C for 3 days. Rabbit and mouse monoclonal antibodies against βIII tubulin (EP1569Y, Abcam, Inc.) and pNF (2F11, EMD MilliporeSigma), respectively, were used at 1:300 dilution. The sample was incubated in the secondary antibody buffer at 4°C for 2 hours. Goat anti-rabbit and anti-mouse IgG antibodies conjugated with Alexa Fluor 594 and Alexa Fluor 647, respectively (Abcam, Inc.), were used. The sample was mounted on a glass slide in Vectashield medium (Vector Laboratories, Inc.). Confocal microscopy was performed with Leica TCS SP8 DLS confocal microscope using an oil-immersion objective lens (HC PL APO CS2 40× 1.3NA, Leica).

Image and statistical analysis. Image processing was done using ImageJ[25] and MATLAB (MathWorks, Inc.). Statistical analysis was performed using MATLAB. Mosaics were created using an ImageJ stitching plugin[26]. SHG normalization and thickness estimation was done as previously described[10]. Briefly, the composite SHG intensity was corrected for topography and normalized by dividing with the Fano factor. The thickness of the retinal nerve fiber was evaluated by means of image segmentation, which consisted of two steps of edge detection and histogram-based thresholding. The thresholded z-stack images were sum-projected and then multiplied with the z-step (2 µm) to obtain the thickness image. Then the SHG density was obtained by dividing the normalized SHG intensity by thickness.

Funding

This work was supported by funding from the National Institute of Health, EY033047 and GM121198 (H.L.).

Authors' Contributions

V.B. performed IOP measurements, tissue preparation, SHG microscopy, and immunohistochemistry; H.L. performed confocal microscopy, analyzed data, and wrote the manuscript; All authors approved the final manuscript.

Competing interests

None.

References

1 Quigley, H. A. & Broman, A. T. The number of people with glaucoma worldwide in 2010 and 2020. *British Journal of Ophthalmology* **90**, 262-267 (2006).

2 Tham, Y. C. *et al.* Global prevalence of glaucoma and projections of glaucoma burden through 2040 A Systematic review and meta-analysis. *Ophthalmology* **121**, 2081-2090, doi:10.1016/j.ophtha.2014.05.013 (2014).

3 Huang, X. R. & Knighton, R. W. Microtubules contribute to the birefringence of the retinal nerve fiber layer. *Investigative Ophthalmology & Visual Science* **46**, 4588-4593 (2005).

4 Huang, X. R., Knighton, R. W. & Cavuoto, L. N. Microtubule contribution to the reflectance of the retinal nerve fiber layer. *Investigative Ophthalmology & Visual Science* **47**, 5363-5367 (2006).

5 Fortune, B., Burgoyne, C. F., Cull, G., Reynaud, J. & Wang, L. Onset and progression of peripapillary retinal nerve fiber layer (RNFL) retardance changes occur earlier than RNFL thickness changes in experimental glaucoma. *Investigative Ophthalmology & Visual Science* **54**, 5653-5660, doi:10.1167/iovs.13-12219 (2013).

6 John, S. W. M. *et al.* Essential iris atrophy, pigment dispersion, and glaucoma in DBA/2J mice. *Investigative Ophthalmology & Visual Science* **39**, 951-962 (1998).

7 Danias, J. *et al.* Quantitative analysis of retinal ganglion cell (RGC) loss in aging DBA/2NNia glaucomatous mice: Comparison with RGC loss in aging C57/BL6 mice. *Investigative Ophthalmology & Visual Science* **44**, 5151-5162 (2003).

8 Libby, R. T. *et al.* Inherited glaucoma in DBA/2J mice: Pertinent disease features for studying the neurodegeneration. *Visual Neuroscience* **22**, 637-648, doi:10.1017/s0952523805225130 (2005).

9 Inman, D. M., Sappington, R. M., Horner, P. J. & Calkins, D. J. Quantitative correlation of optic nerve pathology with ocular pressure and corneal thickness in the DBA/2 mouse model of glaucoma. *Investigative Ophthalmology & Visual Science* **47**, 986-996, doi:10.1167/iovs.05-0925 (2006).

10 Sharoukhov, D., Bucinca-Cupallari, F. & Lim, H. Microtubule imaging reveals cytoskeletal deficit predisposing the retinal ganglion cell axons to atrophy in DBA/2J. *Investigative Ophthalmology & Visual Science* **59**, 5292-5300 (2018).

11 Wang, J. T., Medress, Z. A., Vargas, M. E. & Barres, B. A. Local axonal protection by WldS as revealed by conditional regulation of protein stability. *Proceedings of the National Academy of Sciences of the United States of America* **112**, 10093-10100, doi:10.1073/pnas.1508337112 (2015).

12 Williams, P. A. *et al.* Vitamin B-3 modulates mitochondrial vulnerability and prevents glaucoma in aged mice. *Science* **355**, 756-760, doi:10.1126/science.aal0092 (2017).

13 Williams, P. A. *et al.* Nicotinamide and WLDS act together to prevent neurodegeneration in glaucoma. *Frontiers in Neuroscience* **11**, doi:10.3389/fnins.2017.00232 (2017).

14 Howell, G. R. *et al.* Absence of glaucoma in DBA/2J mice homozygous for wild-type versions of Gpnmb and Tyrp1. *BMC Genetics* **8**, 45, doi:10.1186/1471-2156-8-45 (2007).

15 Pease, M. E., Cone, F. E., Gelman, S., Son, J. L. & Quigley, H. A. Calibration of the TonoLab tonometer in mice with spontaneous or experimental glaucoma. *Investigative Ophthalmology & Visual Science* **52**, 858-864, doi:10.1167/iovs.10-5556 (2011).

16 Lim, H. & Danias, J. Label-free morphometry of retinal nerve fiber bundles by second-harmonic-generation microscopy. *Optics Letters* **37**, 2316-2318 (2012).

17 Lim, H. & Danias, J. Effect of axonal micro-tubules on the morphology of retinal nerve fibers studied by second-harmonic generation. *Journal of Biomedical Optics* **17**, 110502 (2012).

18 Dombeck, D. *et al.* Uniform polarity microtubule assemblies imaged in native brain tissue by second-harmonic generation microscopy. *Proceedings of the National Academy of Sciences of the United States of America* **100**, 7081-7086 (2003).

19 Dieterich, D. C. *et al.* Partial regeneration and long-term survival of rat retinal ganglion cells after optic nerve crush is accompanied by altered expression, phosphorylation and distribution of cytoskeletal proteins. *Eur. J. Neurosci.* **15**, 1433-1443, doi:10.1046/j.1460-9568.2002.01977.x (2002).

20 Soto, I. *et al.* Retinal ganglion cell loss in a rat ocular hypertension model Is sectorial and involves early optic nerve axon loss. *Investigative Ophthalmology & Visual Science* **52**, 434-441 (2011).

21 Jakobs, T. C., Libby, R. T., Ben, Y. X., John, S. W. M. & Masland, R. H. Retinal ganglion cell degeneration is topological but not cell type specific in DBA/2J mice. *Journal of Cell Biology* **171**, 313-325 (2005).

22 Schlamp, C. L., Li, Y., Dietz, J. A., Janssen, K. T. & Nickells, R. W. Progressive ganglion cell loss and optic nerve degeneration in DBA/2J mice is variable and asymmetric. *BMC Neuroscience* **7**, doi:10.1186/1471-2202-7-66 (2006).

23 Howell, G. R. *et al.* Axons of retinal ganglion cells are insulted in the optic nerve early in DBA/2J glaucoma. *Journal of Cell Biology* **179**, 1523-1537 (2007).

24 Savinova, O. V. *et al.* Intraocular pressure in genetically distinct mice: an update and strain survey. *Bmc Genetics* **2**, doi:10.1186/1471-2156-2-12 (2001).

25 Schneider, C. A., Rasband, W. S. & Eliceiri, K. W. NIH Image to ImageJ: 25 years of image analysis. *Nature Methods* **9**, 671-675, doi:10.1038/nmeth.2089 (2012).

26 Preibisch, S., Saalfeld, S. & Tomancak, P. Globally optimal stitching of tiled 3D microscopic image acquisitions. *Bioinformatics* **25**, 1463-1465, doi:10.1093/bioinformatics/btp184 (2009).

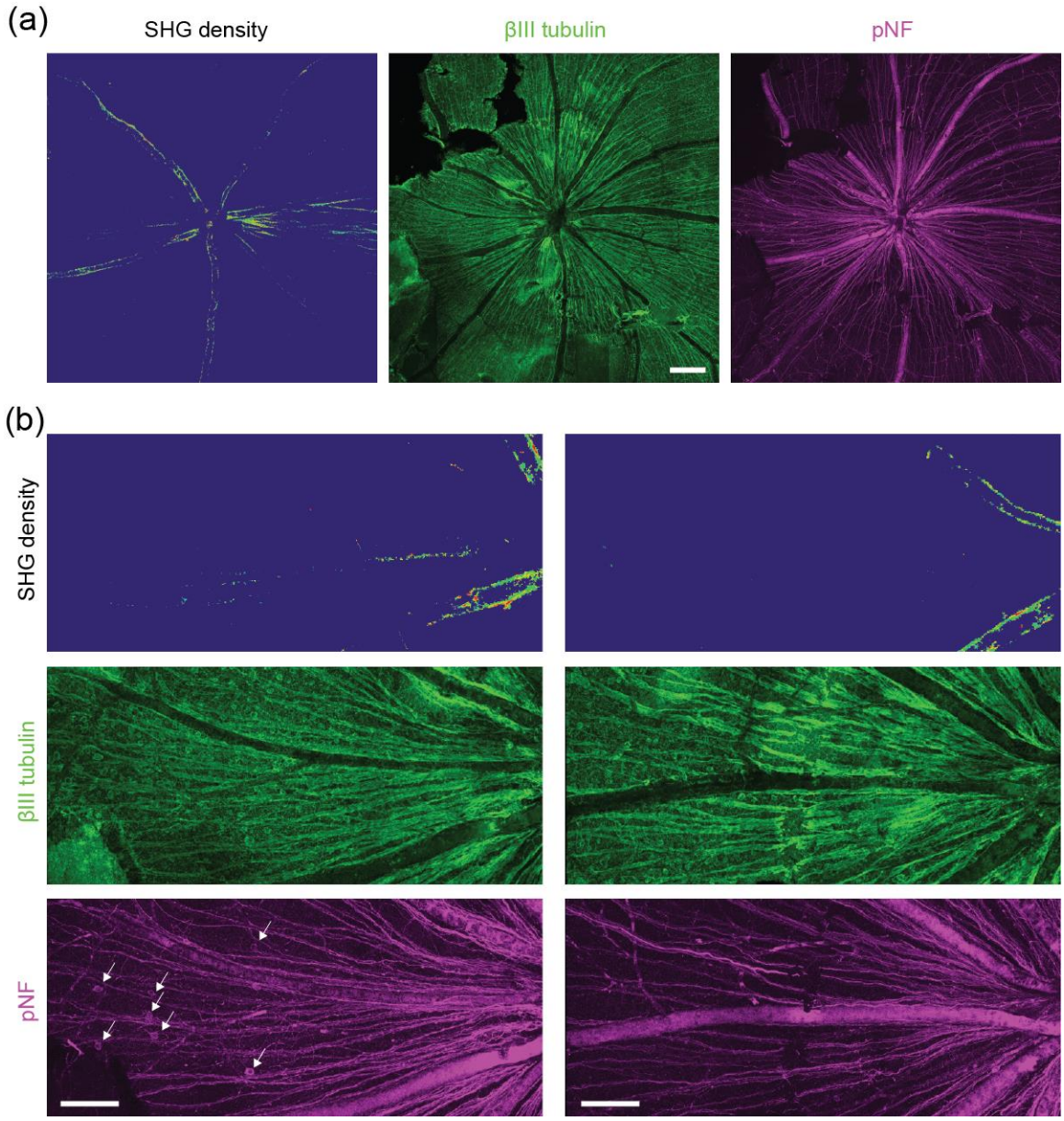

fig. S1. Microtubule deficit versus the distribution of cytoskeletal proteins, βIII tubulin and pNF. (a) Mosaics of a DBA retina (12 months age, female) by SHG and immunofluorescence against the cytoskeletal elements. Scale bars, 200 μm. (b) Comparing two sectors in different stages of RGC degeneration. Arrows, pNF+ RGC somas. Scale bars, 100 μm.